PCCP

Accepted Manuscript

ROYAL SOCIETY OF CHEMISTRY

www.rsc.org/pccp

Cite this: DOI: 10.1039/c0xx00000x

www.rsc.org/xxxxxx

ARTICLE TYPE

Synthesis and microwave absorption characterization of SiO_2 coated Fe_3O_4/MWCNT composites

Hoda Hekmatara*[a], Majid Seifi[a], Keyvan Forooraghi[b], Sharareh Mirzaee[a]

Received (in XXX, XXX) Xth XXXXXXXXX 20XX, Accepted Xth XXXXXXXXX 20XX
DOI: 10.1039/b000000x

This study investigated the microwave absorption properties of core-shell composites containing; iron oxide decorated carbon nanotubes (CNT) and silica (SiO_2@Fe_3O_4/MWCNT) with various thickness of silica shell (7, 20 and 50nm). Transmission electron microscopy (TEM) and X-ray diffraction results confirmed the formation of these core-shell structures. Microwave absorption characterization of the samples at the ranging band under consideration (the X-band) showed increased absorption and shifting of the peaks to lower frequencies compared to uncoated sample (Fe_3O_4/MWCNT). The minimum reflection loss decreased with increasing SiO_2 thickness. The minimum reflection loss of the composite with an optimized thickness of silica shell (7nm) exceeded -41dB at 8.7-9GHz.

Introduction

Worldwide attention has been focused on microwave absorbing materials because microwave absorbing technology is a valuable topic for military purposes and also a rising major issue in the industrial field. In particular, there has been the development of radar absorbing material (RAMs) which can be widely used in the stealth technology of aircraft, microwave dark-rooms and protection[1,2]. In recent years, there have been many attempts to design nano- RAMs, which have suitable factors such as: weight, cost, thickness and biocompatibility. There are a wide range of nanomaterials applied as nano-RAMs[3-6].

The imaginary (ε″) part of complex permittivity is an important parameter which represents the electromagnetic energy loss ability of materials.

If an electromagnetic field propagates in a loss dielectric material, two kinds of electrical currents arise: displacement and conduction currents. The real part of permittivity describes the polarization effect due to the interaction with bound charges (i.e., the displacement current), and the imaginary part describes the effects due to free electron's (conduction current) increase to power loss. The real and imaginary part infers to the storage and loss part of the energy of a material respectively. Since, the MWCNT has free electrons in its skeleton, loading MWCNT inside an epoxy resin leads to increase the values of both imaginary part and real part of permittivity. Increasing the weight ratio of MWCNT, significantly improves the imaginary part of the permittivity in the MWCNT based composites. For example, incorporating 10wt% of MWCNTs inside the epoxy resin of EPON, increase the real and imaginary parts of permittivity range from 67–42 and 76–60 in the frequency of 8.2–12.4 GHz. This value for complex permittivity caused 20 decibels (dB) of attenuation[7-9].

Whereas, CNTs do not show magnetic loss in the microwave absorbing process and their absorption characteristics are limited. The absorption characteristics of carbon nanotubes could be improved by using low decorating ratios of magnetic materials. Sometimes, the magnetic modification of nanotubes results in the enhancement of nanotube composite reflection loss of over 20dB[10-13].

Excellent electromagnetic wave absorption resulted from the efficient complement between the relative permittivity and permeability in materials. Either only the magnetic loss or only the dielectric loss may induce a weak electromagnetic wave absorption property due to the imbalance of the electromagnetic match. In the case of silica-coated iron oxide and MWCNT, a better match of the dielectric loss and magnetic loss may be realized by the existence of the protective silica shell[14,15].

Furthermore, coating magnetic nanoparticles with an insulating material is realized as an effective way to increase the surface anisotropic energy and reduce the eddy current effect. Multi polarization on ferromagnetic/dielectric interfaces may also be conductive to high electromagnetic analysis efficiency[16,17].

The uniform coating of metal nanoparticles with silica shells such as Fe_3O_4 and Fe nanocubes has been reported for microwave absorption with a minimum RL of about -5 and -18.2 dB, respectively. However, a minimum reflection loss lower than -20 dB is required for practical applications[18,19].

In this paper, like the large numbers of work which were reported in the field of producing RAMs, the original proposal is the attenuation of reflected wave to abscond the special surfaces from the radar receivers.

Short circuited method is usually applied for measuring the reflection loss to determine the absorption property of a sample. In this method, the transmitted waves were reflected from a perfect conductor which placed at the end of the sample and gets

back into the sample. So the transparency of material can't be determined by this method. Only the ability of material in losing the reflected wave from its surface is calculated[20,21].

In this work, the Fe_3O_4 decorated MWCNT was prepared using the wet chemical method and then coated with different layer of SiO_2 by a sol-gel process. The resulting core–shell composite (SiO_2@Fe_3O_4/MWCNT) with a thin layer of SiO_2 (7nm) exhibits an excellent absorption property compared to an uncoated sample (Fe_3O_4/MWCNT). Increasing the thickness of the silica coverage leads to a decrement in the microwave absorption and a shifting of the minimum reflection loss to the lower frequencies.

Material and method

Preparation of Fe_3O_4/MWCNT

Iron oxide decorated multiwall CNTs (MWCNT/Fe_3O_4) were produced by mixing 96mg O-MWCNT with 81mg $FeCl_3.6H_2O$ and 120mg $FeCl_2.4H_2O$ in deionized water in an argon atmosphere. The mixture was stirred for 30min and then a diluted solution of ammonia was added drop-by-drop until pH = 12. The synthesis process was followed by heating the mixture to 60°C for 2 h. The product was then washed and air-dried at 50°C.

Preparation of the core-shell structures (SiO_2@Fe_3O_4/MWCNT)

SiO_2@Fe_3O_4/MWCNT composites were prepared by a sol–gel method, similar to the previous report[22]. A quantity of 100 mg as-prepared Fe_3O_4/MWCNT powder was mixed with 100 ml ethanol and the mixture was sonicated for 1 h. 10 ml ethanol and 1 ml tetraethyl silicate (TEOS) was added into the solution and the mixture was stirred for 10 min. This process was followed by the addition of 28 ml NH_4OH drop-by-drop under stirring (1,000 rpm) for 15 h. The resulting product (SiO_2@Fe_3O_4/MWCNT) was then washed with deionized water and dried in an oven at 60°C overnight. The second and third samples were produced by the same protocol and by using different amounts of TEOS (2 ml and 4 ml, respectively).

Reaction process in detail:

$$Si(OC_2H_5) + H_2O \text{ or } C_2H_5OH \text{ (ethanol)} \xrightarrow[\text{Hydrolysis}]{} Si(OH)_4$$

$$Si(OH)_4 \xrightarrow[\text{Condensation at pH=12 \& room temperature}]{} SiO_2$$

In which, the SiO_2 was attached to the hydroxylic functional group of Fe_3O_4 or hydroxylic & carboxylic functional groups of the MWCNT[22].

The morphology of the Fe_3O_4/MWCNT and core-shell structures (SiO_2@Fe_3O_4/MWCNT) was characterized by TEM (PHILIPS MC 10). XRD analysis was carried out on an X-Pert Pro-MPD using CuKα radiation. The room temperature magnetization in the applied magnetic field was performed with a vibrating sample magnetometer (VSM JDM-13). The reflection loss characteristic of all the specimens (with a thicknesses of 4mm) was measured in the 8-12 GHz frequency range (X-band) using an 8822D two port vector network analyser.

Result and discussion

X-ray diffraction

Fig.1 shows the X-ray diffraction pattern of the core-shell structures (SiO_2 coated Fe_3O_4/MWCNT) with different thicknesses of SiO_2 shells. The diffraction peaks of the CNT commonly appear as $2\theta = 26^\circ$ and 32°, while, abroad diffraction peak from $2\theta=22^\circ$ to 28° was assigned to the SiO_2 coverage. This peak is usually observed for SiO_2 coated Fe_3O_4 nanoparticles which were produced using the similar method at room temperature[23,24].

The XRD patterns indicate that by increasing the thickness of the SiO_2 shell, the first peak of the MWCNT and the SiO_2 diffraction peak were combined together gradually. Finally, in Fig. 1c, only one broadened peak could be observed. The other peaks belong to the magnetite (Fe_3O_4) phase which appeared at 36°, 57° and 63° and are attributed to [311], [422] and [511] respectively. Increasing the SiO_2 shell also leads to an increment in the intensity of the SiO_2 peak compared to those of magnetite.

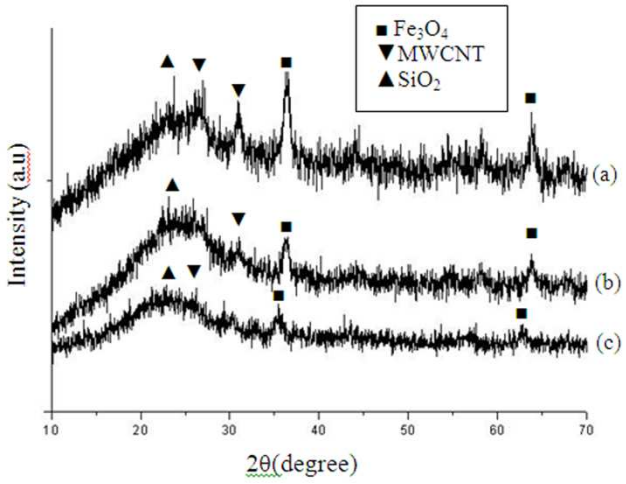

Fig. 1 XRD patterns of SiO_2@Fe_3O_4/MWCNT with different SiO_2 thicknesses of: (a)7nm, (b)20nm and (c)50nm.

Transmission electron microscopy

The TEM images of the Fe_3O_4/MWCNTs and the samples coated with different shell thicknesses of SiO_2 are illustrated in Fig 2. In this work, MWCNTs with an average diameter of 10-20nm and length of 10-30μm were used. The TEM image from the Fe_3O_4 decorated MWCNT sample (Fig. 2a) shows that the Fe_3O_4 nanoparticles were captured in the form of clusters on the CNT's side walls. Each cluster contains a large amount of nanoparticles with a size distribution of 7-18nm. No free nanoparticles were found in the grid.

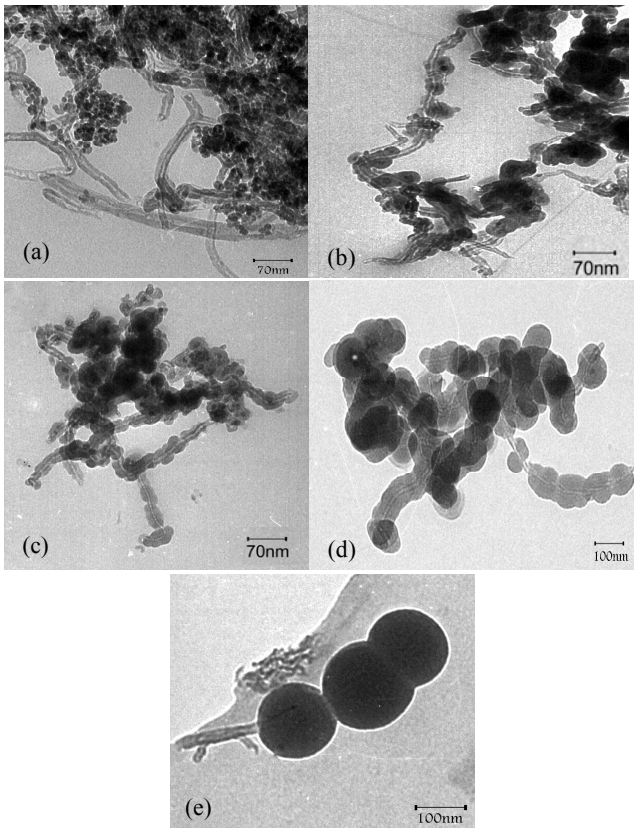

Fig.2 TEM images of: (a) Fe_3O_4/MWCNT and SiO_2@Fe_3O_4/MWCNT with different SiO_2 thicknesses of: (b)7nm, (c)20nm and (d)50nm. (e) an individual Fe_3O_4/MWCNTs which coated with SiO_2 thickness of 50nm and (f) EDS of SiO_2@Fe_3O_4/MWCNT.

The TEM images from the Fe_3O_4/MWCNTs which were coated with different thicknesses of SiO_2 layers show that (except for the sample prepared with the lowest amount of TEOS), the entirety of the CNT's and Fe_3O_4 nanoparticle's surfaces were covered with a homogenous layer of SiO_2 and were composed of a core-shell structure (Figs. 2c and 2d). In the sample with the lowest thickness of SiO_2 (Fig. 2b), only the Fe_3O_4 surface was covered with a silica layer with a thickness of 7nm while the CNT's side walls remained without any coverage. This observation related to the higher reactivity of the Fe_3O_4 nanoparticle's surface than the CNT's walls, as a result of the high number of hydroxyl groups. Increasing the silicate reagent (2ml) leads to covering the surface of the CNTs with a 20nm thickness of SiO_2 (Fig. 2c). With further increments of TEOS (4ml), as shown in Fig. 2d, the thickness of the SiO_2 layer was raised to 50nm. Fig. 2e shows an individual CNT, it can be observed that the anisotropic Fe_3O_4 cluster (Fig. 2a) changes to a smooth and homogenous surface as a result of the SiO_2 coverage.

TGA analysis

Thermal stability of produced composite was investigated using TGA analysis.

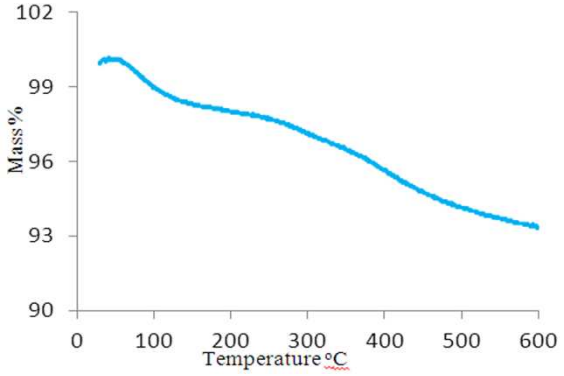

Fig 3. weight loss versus decomposition temperature for SiO_2@Fe_3O_4/MWCNT with SiO_2 thicknesses of 7nm.

The decomposition temperature for all kinds of CNTs is in the temperature range of 400 to 600°C[25]. From TGA curve can be observed that by loading Fe_3O_4 and Silica (SiO_2) on acid-functionalized MWCNT the initial decomposing temperature for SiO_2@Fe_3O_4/MWCNT sample with the lowest thickness of SiO_2 is over 600°C. So the thermal stability of this composite wasn't changed obviously compared to that of the bare MWCNT.

The actual percentage of component in each composite was determined using atomic absorption spectroscopy.

The result shows that the loading of Fe_3O_4 on MWCNTs is 22.5wt% and the weight percentage of SiO_2 in composites with the SiO_2 shell thicknesses of 7, 20 and 50nm is 18%, 34% and 52wt%, respectively.

Vibrating sample magnetometer

The magnetic properties of the Fe_3O_4 decorated MWCNT and SiO_2 coated Fe_3O_4/MWCNT with different thicknesses of SiO_2 shells were investigated with a vibrating sample magnetometer (VSM). Typical magnetization curves as a function of the applied magnetic field at room temperature are shown in Fig. 4.

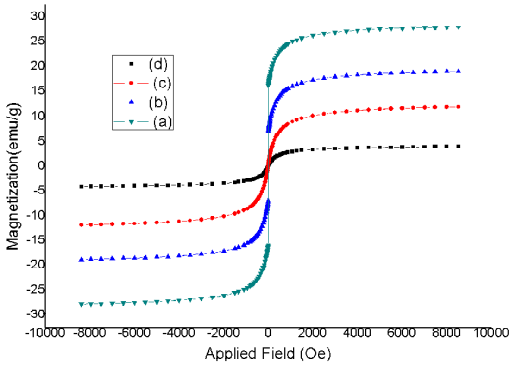

Fig. 4 magnetization curves of: (a) Fe_3O_4/MWCNT and SiO_2@Fe_3O_4/MWCNT with different SiO_2 thicknesses of: (b)7nm, (c)20nm and (d)50nm.

For the Fe_3O_4 decorated MWCNT and all the core-shell structures, there is no pronounced hysteresis loop, which

indicates that both the retentiveness and coerciveness of the composites are zero. This observation is consistent with the superparamagnetic behaviour of the samples. Doping CNTs with a limited size (<20nm) of Fe_3O_4 nanoparticles as superparamagnetic particles caused a high saturation magnetization exceeding 26emu/g. SiO_2 coverage with an almost zero saturation magnetization on the Fe_3O_4 decorated CNTs led to a decrease in the magnetization property[26]. For the core-shell structure, in which only the Fe_3O_4 nanoparticle's surfaces are covered with the SiO_2 shell (Fig. 2b), the saturation magnetization is rapidly increased to 17emu/g. By further increasing the SiO_2 shell thickness (20nm) which coats the entire surface of the nanotubes, the saturation magnetization decreased to 12emu/g. Finally, the weakest magnetization was observed for the sample with the thickest SiO_2 shell (50nm), whereby the saturation magnetization reached up to 2emu/g.

Microwave absorption

The microwave absorption properties of Fe_3O_4/MWCNT and SiO_2@Fe_3O_4/MWCNT core-shell structures with different thicknesses of SiO_2 shells are investigated. The microwave absorption ability of samples with a weight ratio of 0.5, 1 and 2wt% to epoxy resin (EPON 828) was evaluated by measuring their reflection loss.

Our composites have low density, so a large volume of these composites are used as filler to achieve a low weight ratio of them to epoxy resin. For the filler which compressed within the epoxy resin to make the sample with 4mm thickness, it couldn't be possible to enhance the amount of filler. The samples with the filler concentration above 2wt%, was very fragile.

Then, every sample with a thickness of 4mm was poured into a standard X-band waveguide. The electromagnetic fields were generated and recorded by an 8822D two port vector network analyser.

For a single microwave absorbing layer backed by a perfect conductor, the reflection loss of electromagnetic radiation is given by Equation1.

$$R(dB) = 20\log\left|\frac{Z_{in}-1}{Z_{in}+1}\right| \qquad (1)$$

Where Z_{in} is the normalized input impedance:

$$Z_{in} = \sqrt{\frac{\mu_r}{\varepsilon_r}}\tanh\left[j\frac{2\pi}{c}\sqrt{\mu_r\varepsilon_r}fd\right] \qquad (2)$$

μ_r and ε_r are the complex relative permeability and permittivity of the composite medium, c is the velocity of light in free space, f is the frequency and d is the thickness of the absorber[27].

Figs. 5-7 show the reflection loss curves of the SiO_2@Fe_3O_4/MWCNT composites with different thicknesses of SiO_2 layers (7, 20 and 50nm, respectively). Each figure contains 0.5, 1 and 2wt% of filler concentration to epoxy resin (EPON 828) within the frequency range of 8-12GHz.

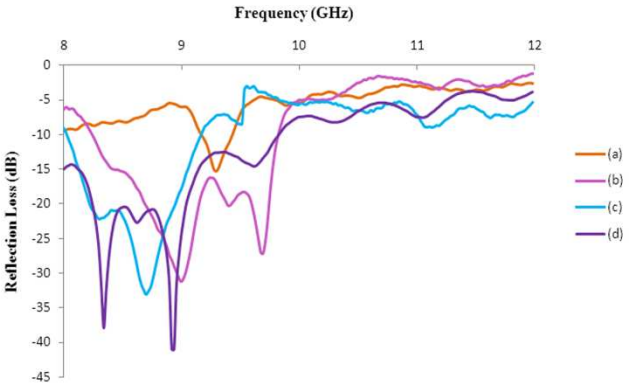

Fig. 5 Reflection Loss curves of: Fe_3O_4/MWCNT (a) and SiO_2 coated Fe_3O_4/MWCNT in thickness of 7nm, with different weight ratio of: 0.5(a), 1(b) and 2(c) to epoxy resin.

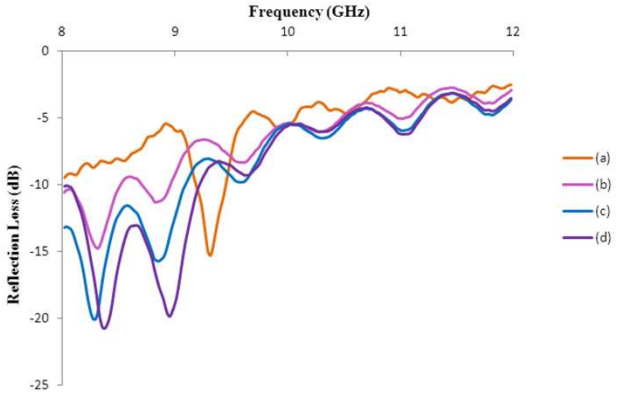

Fig. 6 Reflection Loss curves of: Fe_3O_4/MWCNT (a) and SiO_2 coated Fe_3O_4/MWCNT in thickness of 20nm, with different weight ratio of: 0.5(a), 1(b) and 2(c) to epoxy resin.

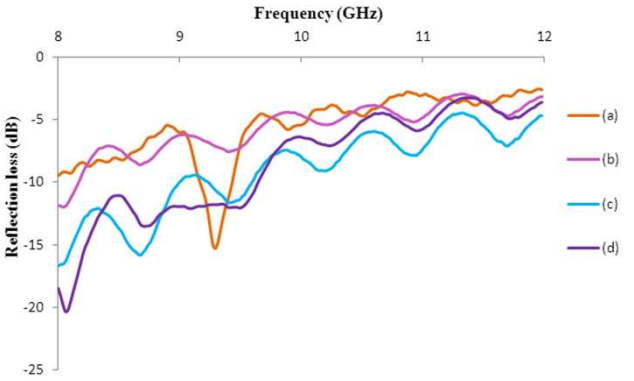

Fig. 7 Reflection Loss curves of: Fe_3O_4/MWCNT (a) and SiO_2 coated Fe_3O_4/MWCNT in thickness of 50nm, with different weight ratio of: 0.5(a), 1(b) and 2(c) to epoxy resin.

It can be observed that, the absorbing curves of all the core-shell structures have two remarkable absorbing peaks. These peaks shifted to a lower frequency range compared to the uncoated sample (Fe_3O_4/MWCNT); this is in agreement with a previous report[28]. It is clear that, the microwave absorption property of the core-shell composites is improved compared to uncoated sample. Moreover, the absorption property of the SiO_2 coated composites is highly dependent on the thickness of the SiO_2 shell. For the composite in which a silica shell covered only the surface of the Fe_3O_4 nanoparticles, an extraordinary

improvement in the minimum reflection loss and bandwidth occurred. In contrast, covering the whole nanotube surface with a thick layer of SiO_2 (50nm) led to a weak absorbing property. An increase in SiO_2 shell thickness also causes a greater peak shifting towards a lower frequency.

Fig. 5 shows that coating the Fe_3O_4 nanoparticles with a SiO_2 layer results in an increment in the microwave absorption property of this composite compared to uncoated sample (Fig. 5a). In this series of samples, both reflection loss and bandwidth increased compared to the uncoated sample. For the concentration of 2wt% of SiO_2@Fe_3O_4/MWCNT to epoxy resin, two minimum reflection losses of -32.7dB and -41dB were observed within the frequency ranges of 8.2-8.4GHz and 8.7-9GHz respectively. Therefore, in comparison with the uncoated sample (Fe_3O_4/MWCNT) in that only one minimum reflection loss is observable, an increment of about 26dB occurred in the reflection loss. The other important point is shown in Fig 6, whereby the absorbing peaks shifted to the lower frequencies and narrower bandwidths by increasing in terms of filler concentrations.

From the curves as shown in Fig. 6, it can be seen that the minimum reflection loss of every sample, increased compared to previous samples with the same concentration (Fig. 5). In the composite with a SiO_2 shell of 20nm in thickness, the reflection loss showed an improvement both in the intensity and the bandwidth compared to the uncoated sample. For instance, the reflection loss of this composite with 2wt% to epoxy resin had two minimums of -20.1dB and -19.6dB with bandwidths of 0.5GHz and 0.4GHz. Meanwhile, at the same concentration, the uncoated sample had one minimum reflection loss of -15.2dB with a bandwidth of 0.4GHz.

Finally, the reflection loss versus frequency for the core-shell composite with the thickest shell (50nm) is illustrated in Fig. 7. At this thickness of SiO_2, the minimum reflection loss shifted to a lower frequency more than before. It may be that, the first minimum reflection loss is placed at lower frequencies below the X band (<8GHz).

Although the stronger absorbing peak was commonly placed at lower frequencies, it is almost impossible to determine definitely how much improvement occurred in the reflection loss. However, in this core-shell composite like the two former samples, the reflection loss is obviously improved compared to similar concentrations of the uncoated sample.

Shielding effectiveness (SE)

EMI shielding effectiveness consists of two mechanisms: reflection and absorption. For reflection of the radiation by the shield, the shield must have mobile charge carriers (electrons or holes) which interact with the electromagnetic fields in the radiation. As a result, the shield tends to be electrically conducting. So metals are by far the most common materials for EMI shielding. They function mainly by reflection due to the free electrons in them. A secondary mechanism of EMI shielding is usually absorption. Loading insulator Fe_3O_4 nanoparticles on MWCNT leads to reduce the electrical conductivity of MWCNT ($\sigma \approx 10^{-8} ohm^{-1} cm^{-1}$) . So the Fe_3O_4 decorated MWCNT showed insulator behaviour. Therefore, our composite expected to have only the shielding effectiveness due to absorption. For significant absorption of the radiation by the shield, the shield should have electric and/or magnetic dipoles which interact with the electromagnetic fields in the radiation. The electric dipoles may be provided by SiO_2 or other materials having a high value of the dielectric constant. The magnetic dipoles may be provided by Fe_3O_4 or other materials having a high value of the magnetic permeability[29-32]. The third shielding mechanism is multiple-reflection; it represents the internal reflections within the shielding material. Typically, multiple-reflection decreases the overall shielding if the shield is thinner than the skin depth and can be ignored if the shield is thicker than the skin depth. The strength of EM wave decreases exponentially as it travels through a conductive material. At a certain distance known as the skin depth the electric field drops to $(1/e)$ of the incident strength, where f is the frequency, $(\mu = \mu_0 \mu_r)$ is the shield's magnetic permeability, μ_0 is equals to $4\pi \times 10^{-7} H/m$, μ_r is the shield's relative magnetic permeability and σ is the shield's electrical conductivity.

The relationship between frequency, electrical conductivity, magnetic permeability and skin-depth is:

$$\delta = 50.33 \times 10^6 (1/f\mu_r\sigma)^{1/2} \qquad (3)$$

For our composite: σ is in the order of 10^{-10}, f is in the order of 10^9 (GHz) and μ_r is in the order of 1. So the skin depth (δ) would be in the order of 10^3 m. Therefore, the thickness of shield (4mm) is much thicker than the skin depth of our composites. So, the multiple-reflection mechanism can be ignored in these materials[33,34].

SE measurement for a typical sample

In order to determine the origin of shielding effectiveness, we measured the shielding effectiveness due to reflection and shielding effectiveness due to absorption for a typical sample which has the lowest minimum reflection loss among the other samples (-41dB at 8.9GHz).

When measurements are made with a network analyser, the shielding effectiveness can be conveniently express in terms of the s-parameters as[29]:

$$SE = 20 * \log|S_{12}| \qquad (4)$$

The total shielding effectiveness and shielding effectiveness due to absorption versus frequency for this sample is shown in Figs.8 and 9, respectively.

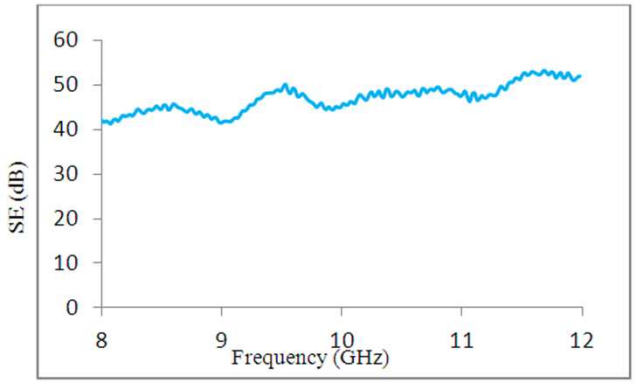

Fig. 8 Total shielding effectiveness (SE) versus frequency, for the sample with minimum reflection loss of -41dB.

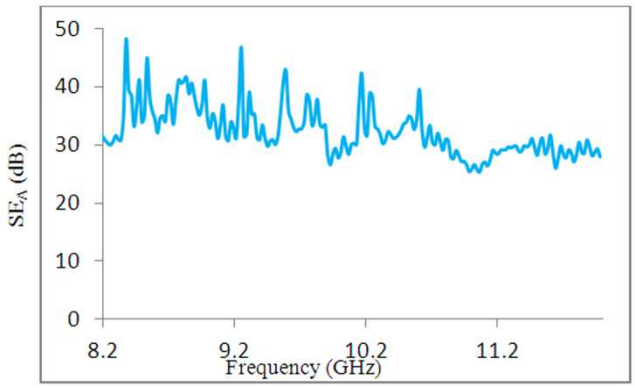

Fig.9 Shielding effectiveness due to absorption (SE_A) versus frequency, for the sample with minimum reflection loss of -41dB.

By ignoring the shielding effectiveness due to multiple-reflection, total shielding effectiveness would be the combination of shielding effectiveness due to absorption and shielding effectiveness due to reflection[30].

$$SE = SE_A + SE_R \qquad (5)$$

As shown in Fig.9, at the frequency of 8.9GHz, in which the lowest minimum reflection loss was observed, the shielding effectiveness due to absorption is 40.2dB and the total shielding effectiveness is 42dB (Fig.8). So shielding effectiveness due to reflection is 1.8dB ($42 = SE_R + 40.2$).

From Figs.8 and 9, it can be seen that the shielding effectiveness due to reflection in some frequencies exceeded less than 1dB.

This result was expected, because our composite have simultaneously electric and magnetic dipoles and majority percentage of shielding effectiveness in these materials is due to absorption[31-34].

Conclusion

SiO_2 coated Fe_3O_4/MWCNT composites with different thicknesses of SiO_2 shells were prepared by a sol-gel method. The microwave absorption properties of these composites were investigated within the frequency range of 8-12GHz. We observed that, the reflection loss of these samples is also highly dependent on the thickness of the SiO_2 coverage.

The best improvement in microwave absorption was observed for the composite in which the SiO_2 shell covered only the surface of the Fe_3O_4 nanoparticles. In this case, free charge polarization can occur between the Fe_3O_4 and the SiO_2 because of the conductivity disparity between the interfaces. Furthermore, covering the Fe_3O_4/MWCNT with a silica shell greatly reduces the eddy current loss and increases the anisotropic energy, which is proven to be crucially important to improving microwave absorption. Enhancing the thickness of the SiO_2 layer on the Fe_3O_4/MWCNT surface leads to a decrement in the absorption property of the composites produced. This result might be related to a reduction of the magnetic loss in these samples as a result of the weaker magnetization property.

Notes and references

[a] *Department of physics, faculty of science Guilan University, Rasht, Iran . Fax: +981313220066; Tel: +981313223132; E-mail:* hd_hekmat@yahoo.com
m_seifi2000@yahoo.com
sharareh_mirzaee@yahoo.com
[b] *Faculty of electrical and computer engineering, tarbiat modares university, Tehran, Iran, Tel: +98912159282; E-mail:* kforooraghi@yahoo.com

1 K.J. Vinoy, R.M. Jha, *Radar Absorbing Materials from Theory to Design and Characterization, Kluwer Academic Publishers,* Boston, 1996.
2 *R.A. Stonier,* SAMPE J, 1991, **27**, 9.
3 M.S. Kim, H.K. Kim, S.W. Byun, S.H. Jeong, Y.K. Hong, J.S. Joo, K.T. Song, J.K. Kim, C.J. Lee, J.Y. Lee, *Synth. Met,* 2002, **126**, 233.
4 R.F. Zhou, H.T. Feng, J.T. Chen, D. Yan, J.J. Feng, H.J. Li, B.S. Geng, S. Cheng, X.Y. Xu, P.X. Yan, *J. Phys. Chem. C*, 2008, **112**, 11767.
5 G.X. Tong, W.H. Wu, J.G. Guan, H.S. Qian, J.H. Yuan, *J. Alloys Compd*, 2011, **509**, 4320.
6 G.X. Tong, J.G. Guan, Z.D. Xiao, X. Huang, Y. Guan, *J. Nanopart. Res.* 2010, **12**, 3025.
7 P. Bhattacharya, S. Sahoo, C. K. Das, *eXPRESS Polymer Letters*, 2013, **7**, 212–223.
8 M. Giorcell, P. Savi, M. Miscuglio, M.Yahya and A. Tagliaferro, *Nanoscale Research Letters*, 2014, **9**,168.
9 E. Decrossas, M. A. El-Sabbagh, V. F. Hanna, and S. M. El-Ghazaly, *electrical engineering and computer science*, 2012, **1**, 1.
10 T. Sameshima, H. Hayasaka and T. Haba, *JJA,* 2009, **48**, 1.
11 L. Chen, Y. Duan, L. Liu, J. Guo, S. Liu, *material and Design.* 2011, **32**, 570.
12 T.J. Imholt, C.A. Dyke, B. Hasslarcher, J.M. Perez, D.W. Price, J.A. Roberts, J.B. Scott, A.Wadhawan, Z. Ye, *J.M. Tour, Chem. Mater,* 2003, **15**, 3969.
13 A. Anand, J.A. Roberts, F. Naab, J.N. Dahiya, O.W. Holland, F.D. McDaniel, *Nucl. Instrum. Meth. B*, 2005, **241** 511.
14 H. Zhou, J. Zhuang, Q. Yan, Q. Liu, *Materials Letters*, 2012, **85**, 117.
15 M. H. Al-Saleh, U. Sundararaj, *CARBON*, 2009, **47**, 1738.
16 J. Zhu, S. Wei, N. Haldolarachige, D.P. Young and Z. Guo, *J. Phys. Chem. C,* 2011, **115**, 15304.
17 X.J. Wei, J.T. Jiang, L. Zhen, Y.X. Gong, W.Z. Shao, C.Y. Xu, *Materials Letters*. 2010, **64**, 57-60.

18 X. Guo, Y. Deng, D. Gu, R. Che, D. Zhao, *J. Mater. Chem.* 2009, **19**, 6706.

19 X. Ni, Z. Zheng, X. Hu, X. Xiao, *J. Colloid Interface Sci.* 2010, **341**, 18.

20 C. Hou, T. Li, T. Zhao, T. Cheng, W. Zhang, G. Li, *Materials Letters*, 2012, **67**, 84–87.

21 H. Hekmatara, M. Seifi, K. Forooraghi, *J. Magn. Magn. Mater,* 2013, **346**, 186–191.

22 X. Ni, Z. Zheng, X. Xiao, L. Huang, L. He, *Materials Chemistry and Physics*, 2010, **120**, 206–212.

23 L. Zhang, H. Zhu, Y. Song, Y. Zhang, Y. Huang, *Materials Science and Engineering B*, 2008, **153**, 78.

24 Y. Mingliang, T. Jiahua, Y. Guanjie, T. Meiyi, Q. Guanzhou, *Trans. Nonferrous Met. Soc. China.* 2010, **20**, 632.

25 D. K. Singh, P. K. Iyer and P. K. Giri, *JOURNAL OF APPLIED PHYSICS*, 2010, **108**, 084313.

26 Y. Sun, L. Duan, Z. Guo, Y. D. Mu, M. Ma, L. Xu, Y. Zhang, N. Gu, *J. Magn. Magn. Mater.* 2005, **285**, 65.

27 M. Guohong, N. Chen, X. Pan, H. Shen, M. Gu, *Mater.Lett.* 2008, **62**, 840

28 R. Han, X. Hua-Han, Li. Qiao, T. Wang, F. Li, *Advanced Materials Research.* 2011, **160**, 957.

29 V. Sadchikov, Z. Prudnikova, Stal.1997, **4**, 66–9.

30 D.D.L. Chung, *Carbon*, 2001, **39**, 279–285.

31 J. Dřínovský, Z. Kejík, *MEASUREMENT SCIENCE REVIEW*, 2009, **9**, 4.

32 C. Morari, I. Balan, J. Pintea, E. Chitanu and I. Iordache, *Progress In Electromagnetics Research M*, 2011, **21**, 93104.

33 M. Baykal, M. Senel, B. Unal, E. Karaog˘lu, H. So¨zeri, M. S. Toprakm, *J Inorg Organomet Polym*, 2013, **23**, 726–735.

34 Z. Liu, G. Bai, Y. Huang, Y. Ma, F. Du, F. Li, *Carbon*, 2007, **45**, 821.